Journal of Alloys and Compounds 509 (2011) 8770–8778

Contents lists available at ScienceDirect

Journal of Alloys and Compounds

journal homepage: www.elsevier.com/locate/jallcom

Formation of zinc aluminum mixed metal oxide nanostructures

Seungho Cho, Kun-Hong Lee*

Department of Chemical Engineering, Pohang University of Science and Technology (POSTECH), San 31, Hyoja-Dong, Nam-Gu, Pohang, Gyungbuk 790-784, Republic of Korea

ARTICLE INFO

Article history:
Received 30 May 2011
Received in revised form 12 June 2011
Accepted 14 June 2011
Available online 21 June 2011

Keywords:
Crystal growth
Zinc oxide
Zinc aluminum oxide
Nanostructures

ABSTRACT

We report a method for synthesizing zinc aluminum layered double hydroxide (ZnAl:LDH) nanostructures at room temperature. The ZnAl:LDH nanoplates could be converted into zinc aluminum mixed metal oxide (MMO) nanostructures by calcination in air. The crystalline nature and morphology of the MMO nanostructures could be tuned by varying the calcination temperature. At low calcination temperatures (450–650 °C), nanostructures were composed of crystalline ZnO regions and amorphous regions. The crystalline orientations of the ZnO crystal grains were almost identical throughout the nanostructure. At calcination temperatures above 750 °C, $ZnAl_2O_4$ crystal grains appeared and amorphous regions could not be found in MMO nanostructures. As the calcination temperature increased, the crystal grain size and surface roughness of MMO nanostructures increased. Calcination at 950 °C resulted in the formation of MMO nanoparticles. The optical properties of the MMO nanostructures were probed by UV–vis diffuse reflectance spectroscopy. The spectra varied depending on their dimensions and crystalline natures.

1. Introduction

Nanomaterials exhibit properties that differ greatly from their bulk counterparts [1–3]. The distinct properties of nanomaterials arise from quantum size effects [4], quantum tunneling effects [5], and surface effects [6]. In addition, the size-dependent properties [7] of nanomaterials render them useful in catalysis [8], electronics [9–11], optics [12,13], chemical sensors [14,15], and information and energy storage [16,17]. In particular, inorganic semiconductor nanostructures are ideal systems for exploring phenomena at the nanoscale for studying the dependence of functional properties on size and dimensionality [18]. They are expected to play key roles in future nanodevices and a variety of applications [19,20]. Performance enhancements can result from tuning the size, morphology and crystalline nature of the semiconductor nanostructures [21–26].

Layered double hydroxides (LDHs) have structures similar to the brucite structure, $Mg(OH)_2$, in which each Mg^{2+} ion is surrounded by six OH^- ions in an octahedral arrangement. LDHs are obtained when a fraction of the divalent cations are isomorphously replaced by trivalent cations [27–29]. The higher charge of the trivalent cations generates an overall positive charge in the brucite-type layers, which is balanced by intercalation of interlayer anions. The general formula of LDH compounds is $[M^{II}_{(1-x)}M^{III}_{(x)}(OH)_2][A^{m-}_{x/m}{\bullet}nH_2O]$ (M^{II} = Zn, Mg, Co, Ni, Fe; M^{III} = Al, Cr, Ga; A = CO_3^{2-}, Cl^-, NO_3^-, CH_3COO^-) [27]. LDHs have good anion exchange capacities, and a wide range of molecules can be introduced into the interlayer. Thus, they have been used in various practical applications, such as anion exchangers [30], catalyst supports [31], electroactive materials [32], and nanocomposites [33]. In addition to their useful practical characteristics, LDHs may be used as precursors for the preparation of mixed metal oxides (MMOs), which can be used as multi-functional materials.

Zinc oxide (ZnO, space group = $P6_3mc$; a = 0.32495 nm, c = 0.52069 nm), which constitutes a new generation semiconductor material, is a II–VI semiconductor with a wide direct band gap of 3.37 eV at room temperature and a large exciton binding energy of approximately 60 meV. ZnO has useful characteristics, such as a large piezoelectric constant, and its electrical conductivity can be easily modified. ZnO has received considerable attention over the past few years because of these unique properties, and has been used in a variety of applications [34–42]. Zinc aluminum oxide ($ZnAl_2O_4$, space group = $Fd3m$; a = 0.80872 nm) has a high thermal stability, high mechanical resistance, hydrophobicity, low surface acidity, and a wide band gap (3.8 eV) [43–45]. It can be used as a transparent conductor, catalyst, catalyst support, polymer electrolyte, and optical coating, and may be used in

* Corresponding author. Tel.: +82 54 279 2271; fax: +82 54 279 5949.
E-mail address: ce20047@postech.ac.kr (K.-H. Lee).

0925-8388/$ – see front matter © 2011 Elsevier B.V. All rights reserved.
doi:10.1016/j.jallcom.2011.06.057

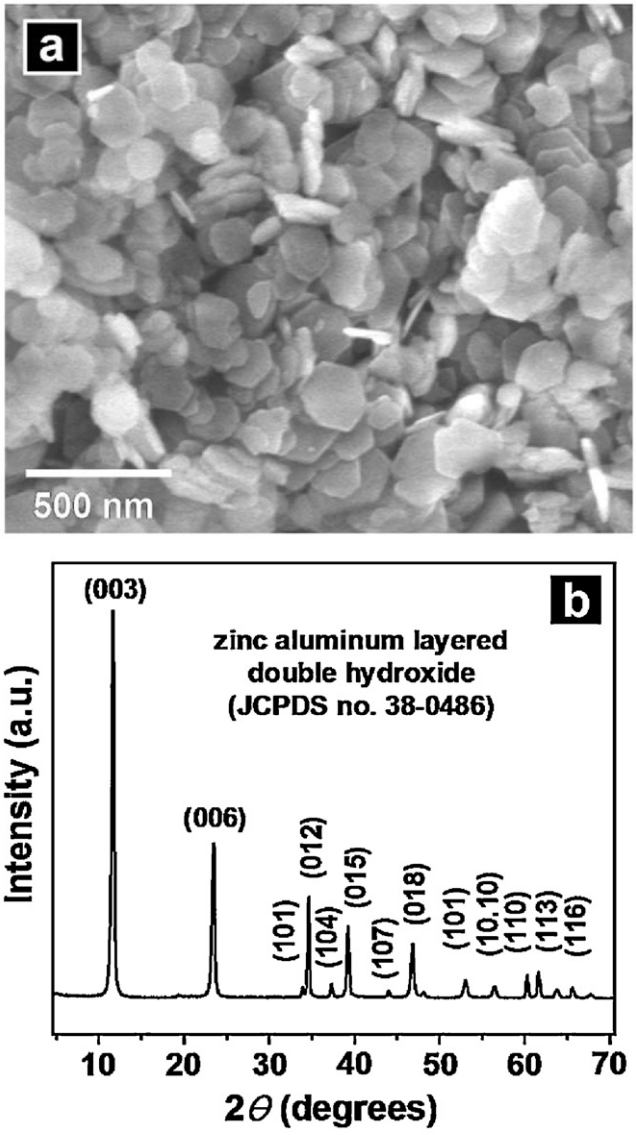

Fig. 1. (a) SEM image and (b) XRD pattern of the structures synthesized by reaction of an aqueous solution containing 0.01 M zinc acetate dihydrate, 0.0033 M aluminum chloride and 0.35 M ammonia at room temperature for 24 h.

applications designed for dehydration, dehydrogenation, and high temperatures [46–55]. Therefore, zinc aluminum MMOs, which are composed of ZnO and $ZnAl_2O_4$, have the potential to be used in a variety of applications. Zinc aluminum MMOs can be used to complement the properties of each component (ZnO or $ZnAl_2O_4$). For example, because both ZnO and $ZnAl_2O_4$ have wide band gap energies and photocatalytic activities, their MMOs may be used as stable optical coating materials, UV absorbers, or photocatalysts for pollutant decomposition or water splitting [56].

In general, the lateral dimensions of zinc aluminum LDHs (ZnAl:LDHs) used as precursors for obtaining zinc aluminum MMOs are large. Under some reaction conditions, the lateral size exceeds the micrometer scale [56–59]. These ZnAl:LDHs, usually prepared by hydrothermal reactions, are too large to use for the preparation of zinc aluminum MMO nanostructures. Slow growth kinetics at room temperature can reduce not only the amount of energy required for fabrication, but also the size of the ZnAl:LDH particles. In some methods used to obtain ZnAl:LDHs, low pressure deposition processes, such as thermal evaporation, atomic layer deposition, or radio frequency magnetron sputtering techniques, have been used to prepare aluminum thin films for aluminum source [57,58]. These processes are energy-intensive and require specialized equipment. In addition, the relationship between the calcination temperature and the morphology and crystalline nature of zinc aluminum MMO nanostructures has not been described previously. In this paper, we report a very simple method for synthesizing ZnAl:LDH nanostructures at room temperature, and we describe their conversion to zinc aluminum MMO nanostructures. The crystalline nature and morphology of MMO nanostructures may be controlled simply by varying the calcination temperature between 450 °C and 950 °C. This method is simple and does not require complex experimental procedures or complicated devices. UV–vis diffuse reflectance spectra of ZnAl:LDH nanostructures and their calcined nanostructures will also be discussed.

2. Experimental

2.1. Preparation of ZnAl:LDH nanostructures

All chemicals used in this study were analytical grade and were used without further purification. An aqueous solution containing 0.01 M zinc acetate dihydrate

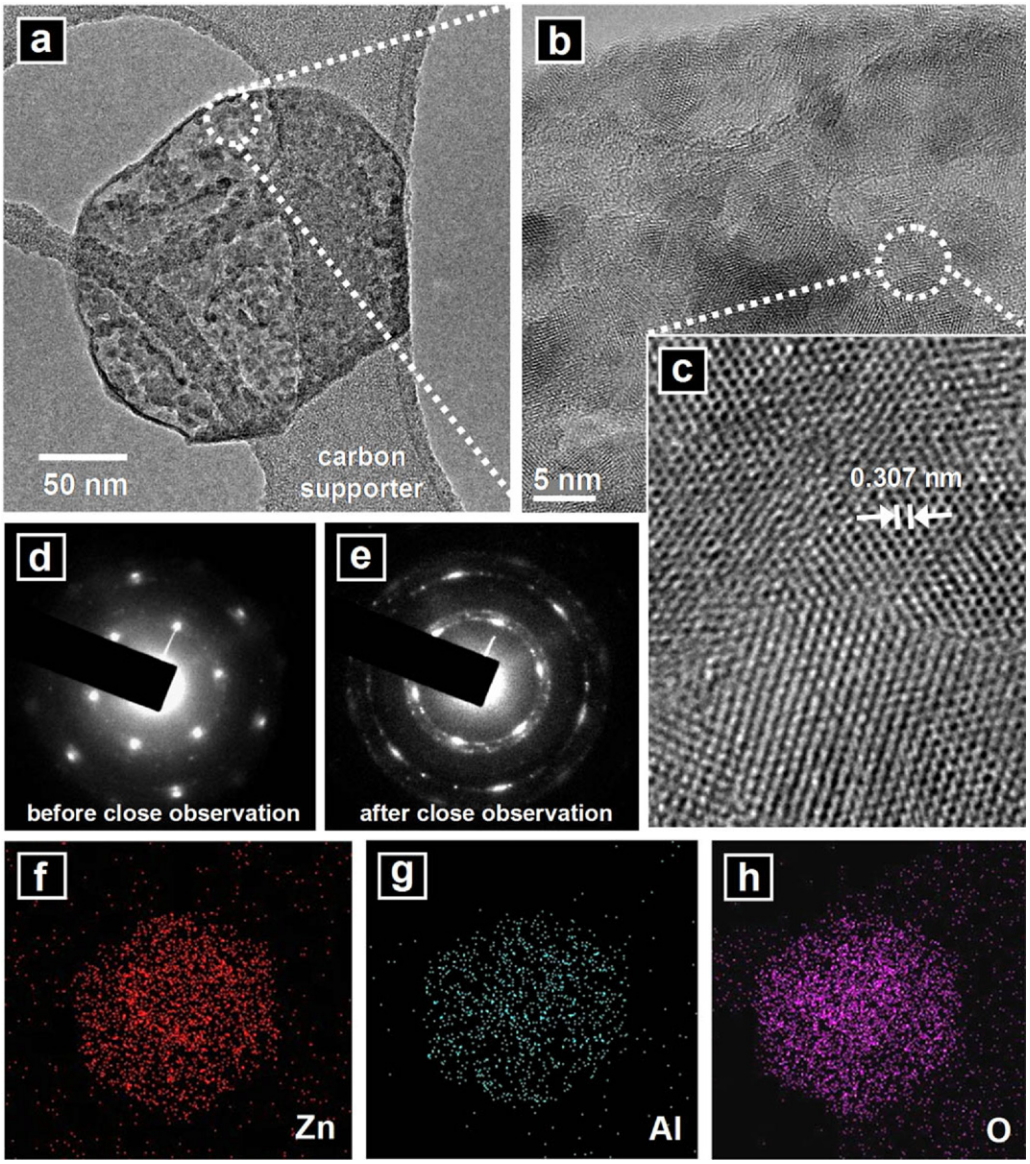

Fig. 2. (a), (b), and (c) show TEM images of a structure synthesized from the reaction of an aqueous solution containing 0.01 M zinc acetate dihydrate, 0.0033 M aluminum chloride, and 0.35 M ammonia at room temperature for 24 h. (d) SAED pattern of the structure prior to HR-TEM imaging. (e) SAED pattern of the structure prior to HR-TEM imaging. (f) Elemental mapping of Zn. (g) Elemental mapping of Al. (h) Elemental mapping of O.

($Zn(CH_3COO)_2{\bullet}2H_2O$, 99%, Samchun), 0.0033 M aluminum chloride ($AlCl_3$, 99.99%, Aldrich), and 0.35 M ammonia (NH_3, Samchun) was prepared and maintained at room temperature for 24 h. After reaction, the solution was filtered through a polycarbonate membrane filter (ISOPORE). The filtered powders were washed several times with deionized water then dried in an oven at 60 °C for 12 h.

2.2. Synthesis of MMO nanostructures

The as-prepared ZnAl:LDH powders were placed in an annealing furnace and maintained at a fixed temperature (450–950 °C) for 2 h in air. After calcination, the powders were removed from the furnace and characterized.

2.3. Characterization

The morphology, crystallinity, crystalline nature, chemical composition, functional groups and optical properties of the samples were determined by field-emission scanning electron microscopy (SEM, JEOL JMS-7401F, operating at 10 keV), X-ray diffraction spectrometry X-ray diffraction (XRD, Mac Science, M18XHF by scanning the 2θ range between 5° and 80° using Cu Kα ($\lambda = 0.15406$ nm) radiation), high-resolution scanning transmission electron microscopy (Cs-corrected HR-STEM, JEOL JEM-2200FS with an energy-dispersive X-ray (EDX) spectrometer operated at 200 kV), inductively coupled plasma atomic emission spectroscopy (ICP-AES, Thermo Elemental, IRIS Advantage), Fourier transform infrared spectroscopy (FT-IR, Jasco Valor-II spectrometer) and UV–vis diffuse reflectance spectroscopy (Shimadzu, UV2501PC).

3. Results and discussion

Fig. 1(a) shows an SEM image of structures synthesized from the reaction of an aqueous solution containing 0.01 M zinc acetate dihydrate, 0.0033 M aluminum chloride and 0.35 M ammonia at room temperature for 24 h. The mild room temperature reaction permitted synthesis of hexagonal nanoplates. The lateral dimensions of the thin plates were 70–200 nm. The crystalline phases of the synthesized powder were determined by XRD analysis. Fig. 1(b) shows an XRD pattern of the powder. The diffraction peaks are typical of LDH structures [60]. The pattern could be indexed as a hexagonal lattice with $R\bar{3}m$ rhombohedral symmetry, which is commonly used to describe LDH structures (JCPDS No. 05-0669) [61]. Parameter a represents the average intermetallic distance calculated from the position of the (1 1 0) reflection and parameter c corresponds

to $3/2(d_{003}+2d_{006})$. Thus, the calculated lattice constants were $a=0.3074$ nm and $c=2.280$ nm. No peaks corresponding to any other phases or impurities were detected, indicating that the precipitates were pure ZnAl:LDHs.

Fig. 2(a) shows a typical low-magnification TEM image of a ZnAl:LDH nanostructure. The surface of the structure was not smooth. Fig. 2(b) shows a higher magnification TEM image of the area indicated by the circle in Fig. 2(a). XRD analysis revealed that it was crystalline in structure. Fig. 2(c), a HR-TEM image of the area marked by a circle in Fig. 2(b) shows that the ZnAl:LDHs were highly crystalline with a lattice spacing of 0.307 nm, which corresponded to the average distance between adjacent hydroxyl groups within layers. The selected-area electron diffraction (SAED) pattern of the structure collected prior to taking HR-TEM images exhibited hexagonally arranged spots, which confirmed that the ZnAl:LDHs were quasi single-crystalline (Fig. 2(d)). However, the SAED pattern obtained after close observations revealed ring-shaped patterns, which indicated that the ZnAl:LDH became poly-crystalline (Fig. 2(e)). During HR-TEM observations, it could be observed that in situ movement of the crystal grains, resulting in polycrystalline structures. During the collection of high resolution electron micrographs, a high energy electron beam was introduced to a unit area of the sample and was found to produce rearrangements in the crystal lattice. Qualitative analysis of the ZnAl:LDH structures was conducted in the scanning transmission electron microscope mode using EDX. The results clearly showed that Zn, Al, and O elements were distributed homogeneously through the entire ZnAl:LDH structure (Fig. 2(f), (g), and (h), respectively). Quantitative chemical analysis using ICP-AES revealed that the ZnAl:LDH had an average Zn/Al molar ratio of 2.49.

The structure of ZnAl:LDHs and an octahedral unit are shown in Fig. 3(a). The octahedral units of Zn^{2+} or Al^{3+} (Zn^{2+}/Al^{3+} atomic ratio of 2.49, 6-fold coordination to OH^-) shared edges to form micrometer-sized inorganic sheets. The higher charge of Al^{3+} generated an overall positive charge in the brucite-type layers, which was balanced by intercalation of interlayer anions. These sheets were stacked on top of each other and held together by hydrogen bonding. In the characterization of LDHs, FT-IR spectroscopy is typically used to analyze the vibrations of octahedral lattice, hydroxyl groups and interlayer anions [62]. The FT-IR spectrum of the ZnAl:LDH nanostructures (Fig. 3(b)) included a broad band at 3350–3500 cm^{-1}, which was attributed to the O–H stretching vibrations associated with the hydrogen bonded network of the in-layer hydroxyl groups and the interlayer water molecules [63]. A band was also observed at 1358 cm^{-1}. This feature was attributed to the vibrations of the interlayer CO_3^{2-} [64]. The spectrum did not contain bands corresponding to the asymmetric (1600 cm^{-1}) and symmetric (1400 cm^{-1}) RCO_2^- stretches, which demonstrates that there are no acetate anions in the interlayer region [59,65,66]. The location of the 0 0 6 peak ($2\theta=23.36^\circ$) in the XRD pattern, shown in Fig. 1(b), indicated that the intercalated anions were composed of both CO_3^{2-} and Cl^-, the latter of which originated from aluminum chloride [67]. As presented in the TEM analysis of the ZnAl:LDH nanostructures (Fig. 2), the crystal structures of ZnAl:LDH were unstable. Because the brucite-type layers were stacked and held together by hydrogen bonding, each layer could be easily moved and reconstructed under application of heat or light. Thus, LDHs were easily converted into MMO upon calcination. In general, precursor ZnAl:LDH structures are synthesized by hydrothermal methods [56,59]. High reaction temperatures lead to fast growth kinetics, which produces relatively large crystals, up to several micrometers in lateral dimensions. Small mother ZnAl:LDH nanostructures are essential for synthesizing zinc aluminum MMO nanostructures.

As illustrated in Fig. 4, ZnAl:LDH nanoplates synthesized under room temperature reaction conditions were filtered, dried, and

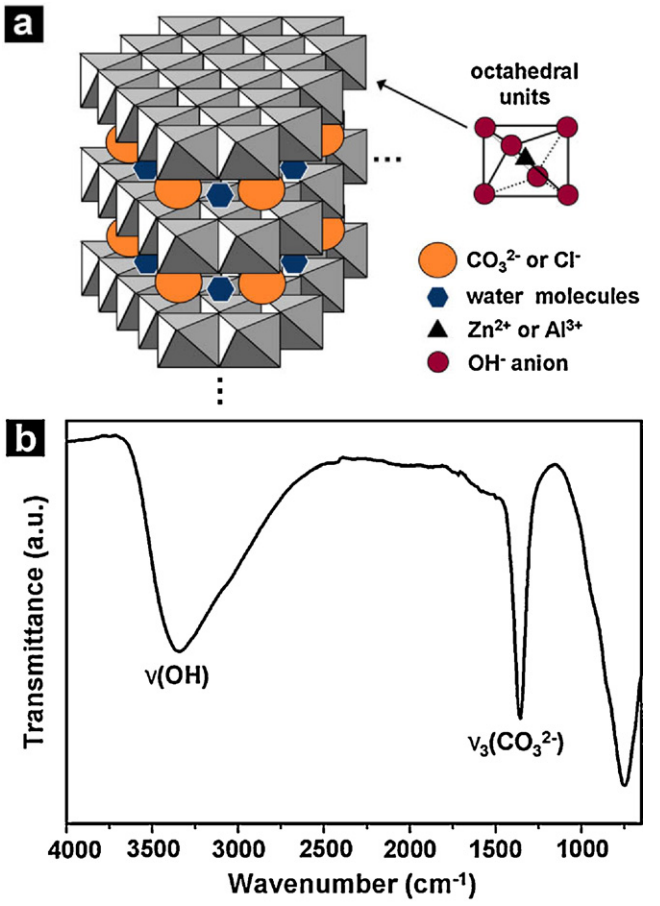

Fig. 3. (a) Schematic diagram of the ZnAl:LDH structures [62]. (b) FT-IR absorption spectrum of powders synthesized in an aqueous solution containing 0.01 M zinc acetate dihydrate, 0.0033 M aluminum chloride, and 0.35 M ammonia at room temperature for 24 h.

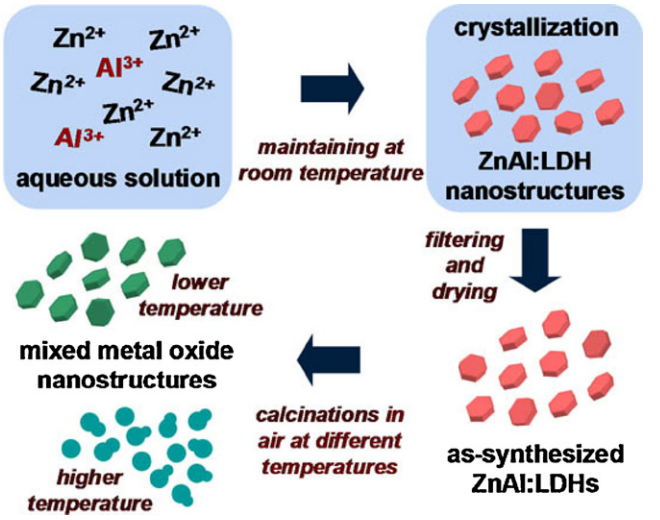

Fig. 4. Schematic illustration of the experimental procedure for the room temperature synthesis of ZnAl:LDH nanostructures and the conversion of the as-prepared ZnAl:LDH nanostructures to zinc aluminum MMO nanostructures by calcination.

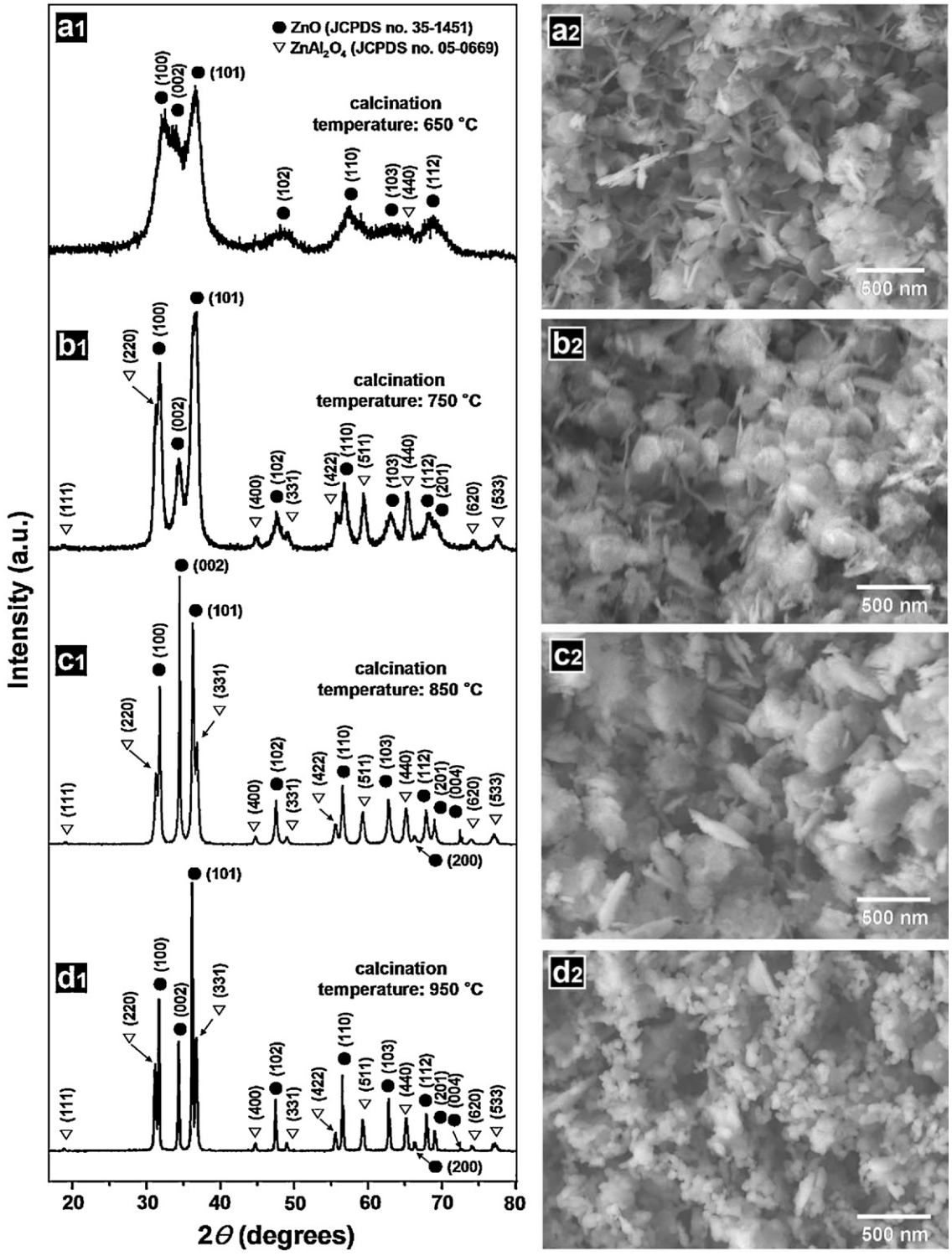

Fig. 5. (a1) XRD pattern and (a2) SEM image of powders obtained by calcination of as-prepared ZnAl:LDH nanostructures at 650 °C for 2 h in air. (b1) XRD pattern and (b2) SEM image of powders obtained by calcination of ZnAl:LDH nanostructures at 750 °C for 2 h in air. (c1) XRD pattern and (c2) SEM image of powders obtained by calcination of ZnAl:LDH nanostructures at 850 °C for 2 h in air. (d1) XRD pattern and (d2) SEM image of powders obtained by calcination of ZnAl:LDH nanostructures at 950 °C for 2 h in air.

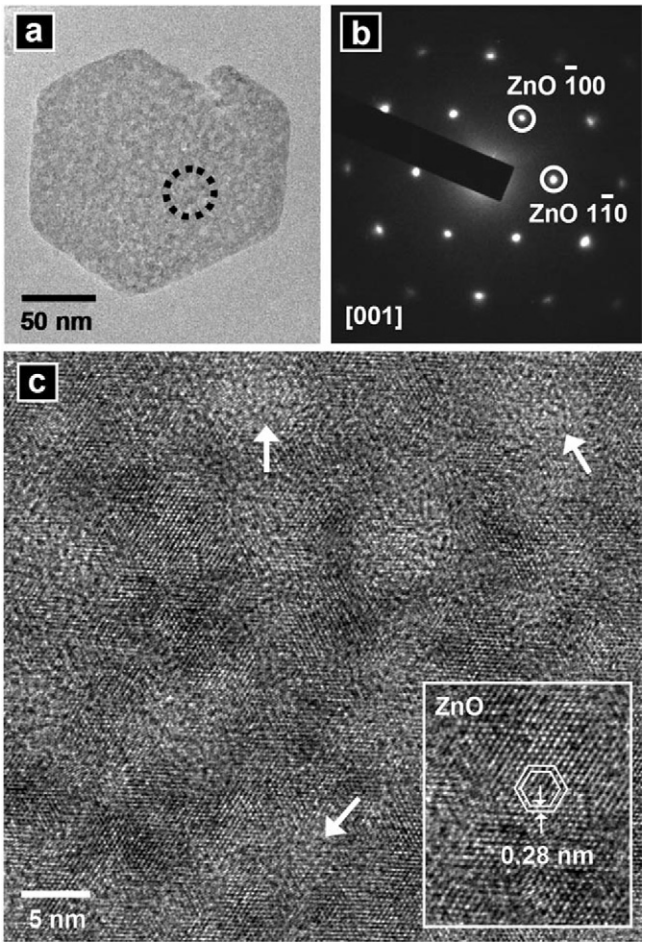

Fig. 6. (a) TEM image of a structure obtained by calcination of as-prepared ZnAl:LDH nanostructures at 650 °C for 2 h in air. (b) SAED pattern of the structure. (c) HR-TEM image of the area indicated by the circle in (a). The inset shows a higher-magnification image of a ZnO crystal grain.

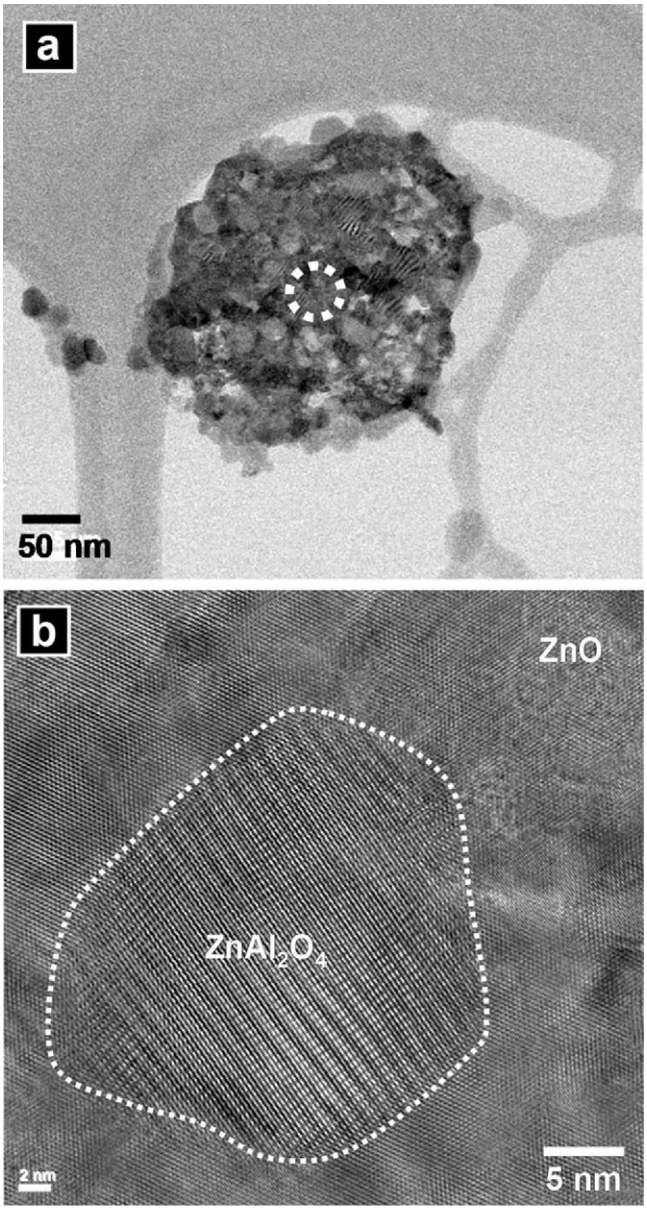

Fig. 7. (a) TEM image of a structure obtained by calcination of as-prepared ZnAl:LDH nanostructures at 750 °C for 2 h in air. (b) HR-TEM image of the area indicated by the circle in (a).

calcined at a fixed temperature for 2 h in air. The calcination temperatures ranged from 450 to 950 °C. At calcination temperatures between 450 °C and 650 °C, the calcined nanostructures had similar morphologies and crystalline natures. Fig. 5(a1) displays the XRD pattern of the products of calcination at 650 °C for 2 h in air. The ZnAl:LDH peaks (Fig. 1(b)) disappeared and new broad peaks emerged as a result of calcination. These new peaks could be indexed as a wurtzite ZnO phase (JCPDS No. 35-1451). The crystalline phase of ZnAl:LDH disappeared, and small ZnO crystal grains grew in the structures. The crystallite size was calculated using Scherrer's equation. The crystallite size of ZnO was about 4.6 nm. SEM imaging (Fig. 5(a2)) showed that the product of calcination at 650 °C almost exactly preserved the shape of the mother ZnAl:LDH nanostructures and yielded a thin plate morphology. Fig. 5(b1) shows the XRD pattern of the products of calcination at 750 °C for 2 h in air. The wurtzite ZnO peaks were sharper than those of the products of calcination at 650 °C, and the cubic $ZnAl_2O_4$ crystalline phase could also be indexed (JCPDS No. 05-0669). The calculated crystallite sizes of ZnO and $ZnAl_2O_4$ were about 8.1 nm and 15.9 nm, respectively. Thus, the size of ZnO crystal grains increased, and $ZnAl_2O_4$ crystal grains also grew in the structures. Fig. 5(b2) shows an SEM image of the nanostructures produced by calcination at 750 °C for 2 h in air. The structure size was almost the same as the size of the mother ZnAl:LDH nanoplates. However, the surface of the product became rougher. The XRD pattern of the products of calcination at 850 °C for 2 h (Fig. 5(c1)) showed that the crystal grain sizes of ZnO (about 36.2 nm) and $ZnAl_2O_4$ (about 46.8 nm) increased. The intensity of the ZnO (002) peak was relatively high. SEM imaging (Fig. 5(c2)) revealed that the plate-like particle shapes were retained but the size of the nanoplates increased relative to the size of the mother ZnAl:LDH nanostructures. Anisotropic powder packing was probable because the structures calcined at 850 °C were larger and had plate-like shapes. The basal planes of a large portion of the MMO crystals were nearly parallel to the flat surface of the substrate (the powder holder for XRD). Thus, the intensity ratio between the ZnO (1 0 0) and ZnO (0 0 2) XRD peaks from products calcined at 850 °C (Fig. 5(c1)) was low. The XRD pattern of the products of calcination at 950 °C for 2 h (Fig. 5(d1)) showed very sharp peaks, indicating a further increase in the crystal grain sizes of ZnO (about 43.7 nm) and $ZnAl_2O_4$ (about 56.2 nm). The intensity ratio of the ZnO (1 0 0) and ZnO (0 0 2) XRD peaks in this sample was higher than that of the sample calcined at 850 °C. An SEM image of

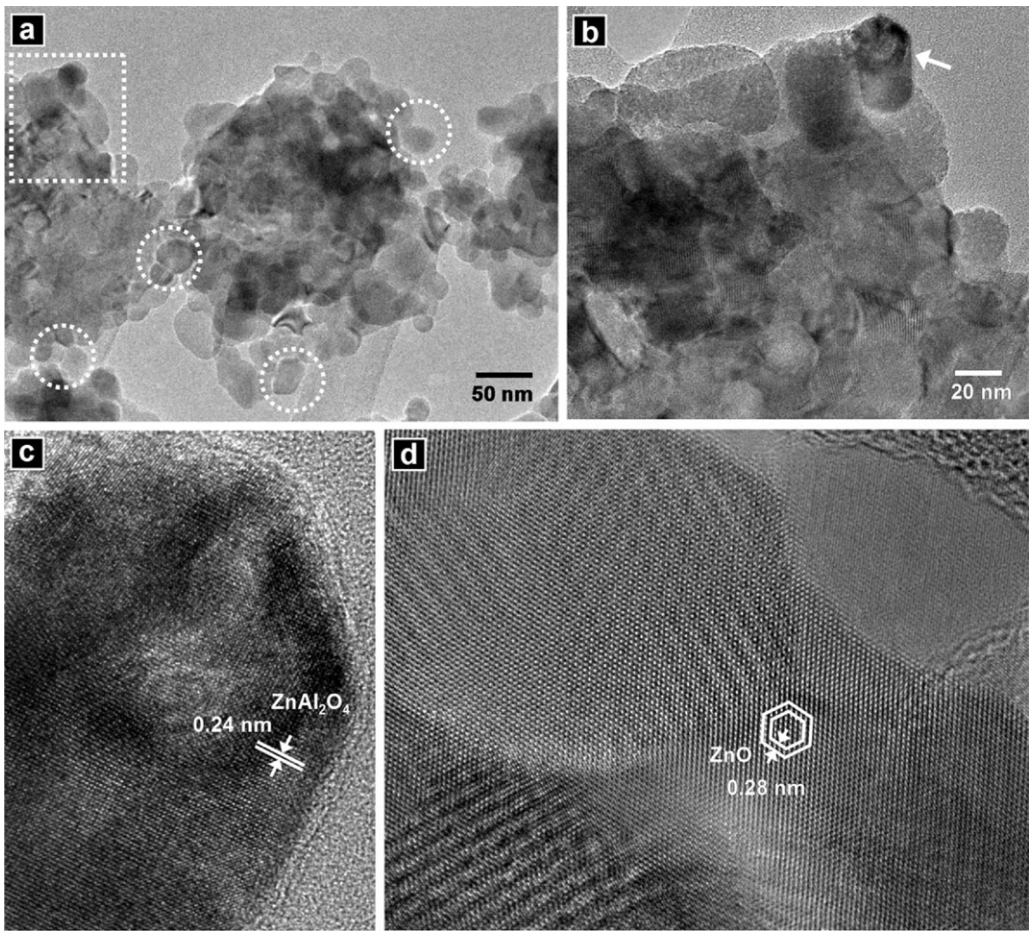

Fig. 8. TEM images of structures obtained by calcination of as-prepared ZnAl:LDH nanostructures at 850 °C for 2 h in air: (a) low magnification, (b) mid magnification, and (c and d) high magnification.

the products calcined at 950 °C (Fig. 5(d2)) revealed powders composed of nanoparticles. The high temperature promoted breaking of the ZnAl:LDH nanoplates, resulting in MMO nanoparticles. Thus, the random orientations of the crystal structures resulted in a high intensity ratio between the ZnO (1 0 0) and ZnO (0 0 2) XRD peaks (Fig. 5(d1)).

The crystalline natures of the calcined products were investigated by collecting magnified TEM images. Fig. 6(a) shows a low-magnification TEM image of a nanostructure produced by calcination at 650 °C for 2 h in air. As shown in the SEM image (Fig. 5(a2)), the resulting nanostructure preserved the hexagonal shape of the mother ZnAl:LDH nanostructure (Fig. 6(a)). Fig. 6(b) shows a SAED pattern of the hexagonal structure shown in Fig. 6(a). Hexagonally arranged regular spots indexed as wurtzite ZnO crystal structures indicated that the crystal orientations of the ZnO crystal grains were almost the same throughout the nanostructure. Thus, the resulting calcined products were influenced by the crystal symmetry and orientation of the ZnAl:LDH nanostructures. The HR-TEM image (Fig. 6(c)) of the area marked by the circle in Fig. 6(a) revealed that the nanostructure was composed of ZnO crystalline and amorphous areas, indicated by the arrows in Fig. 6(c). The inset of Fig. 6(c) shows a high magnification image of a ZnO crystal grain with a lattice spacing of 0.28 nm that corresponded to interspacings of the {1 0 0} planes in the ZnO crystal lattice. Qualitative EDX analysis detected the presence of Al elements. We propose that these Al elements may be present predominantly in the amorphous areas.

Fig. 7(a) shows a low-magnification TEM image of a nanostructure produced by calcination at 750 °C for 2 h in air. The surface of the nanostructure was much rougher than the surfaces of calcination products prepared at 650 °C. The products maintained hexagonally shaped plates. $ZnAl_2O_4$ crystal grains could be found, as shown in the HR-TEM image (Fig. 7(b)), which was consistent with the XRD results (Fig. 5(b1)). Amorphous regions could not be found in the nanostructures. Fig. 8 shows TEM images of the structures produced by calcination at 850 °C for 2 h in air. The nanoplate structures became rougher, and some nanoparticles appeared to leave the main plate-like nanostructures, as indicated by the circles in Fig. 8(a). Fig. 8(b) shows a high-magnification TEM image of the area marked by the rectangle in Fig. 8(a). HR-TEM images showed that the nanoplates were composed of $ZnAl_2O_4$ crystal grains (Fig. 8(c)) and ZnO crystal grains (Fig. 8(d)). Fig. 8(c) shows that the crystal grains had a lattice spacing of 0.24 nm, corresponding to the distance between the (311) planes in the $ZnAl_2O_4$ crystal lattice. Fig. 8(d) shows that the ZnO crystallite had a lattice spacing of 0.28 nm, which corresponded to the distance between the {1 0 0} planes in the ZnO crystal lattice. The crystal grain sizes of the nanostructures were larger than the grain sizes of products prepared at lower calcination temperatures. Fig. 9(a) shows a TEM image of the products calcined at 950 °C. High energy applied to ZnAl:LDH resulted in formation of MMO nanoparticles during the calcination process. HR-TEM images (Fig. 9(b)) of the area indicated by the circle in Fig. 9(a) showed that the nanoparticles were highly crystalline, with a lattice spacing of 0.28 nm, which corresponded to the distance between {1 0 0} planes in the ZnO crystal lattice. HR-TEM analysis revealed that most individual nanoparticles were single crystalline.

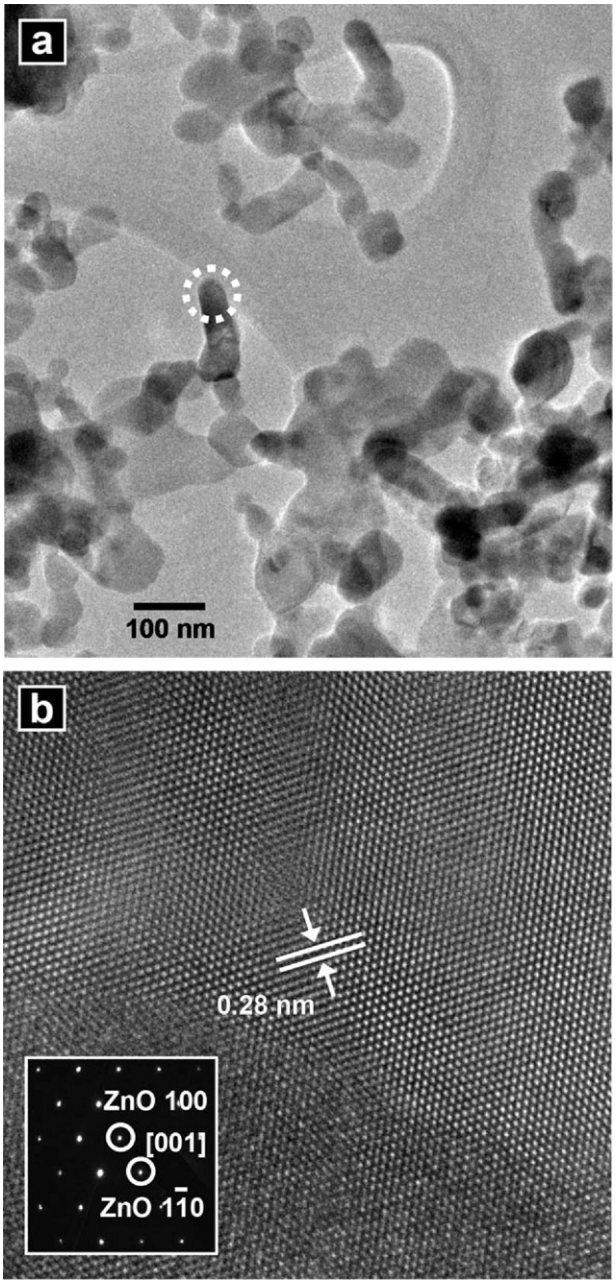

Fig. 9. (a) TEM image of structures obtained by calcination of as-prepared ZnAl:LDH nanostructures at 950 °C for 2 h in air. (b) HR-TEM image of the nanoparticle indicated by the circle in (a). The inset shows the SAED pattern of the nanoparticle.

The UV–vis diffuse reflectance spectra of the ZnAl:LDH nanostructures and their calcined nanostructures are presented in Fig. 10. ZnAl:LDH nanostructures did not absorb UV and visible light. Nanostructures prepared by calcination at 450 °C for 2 h in air absorbed in the ultraviolet region. As the calcination temperature increased from 450 °C to 650 °C, the UV absorbance spectrum of the nanostructures gradually shifted toward longer wavelengths because the nanostructures included smaller amorphous areas and larger crystalline grains. Above 750 °C, the calcined MMO nanostructures showed broad strong absorptions in the near-ultraviolet region, which were characteristic of ZnO and $ZnAl_2O_4$ wide band gap semiconductor materials. No amorphous regions were present in the MMO nanostructures, and the nanostructures had good crystallinity, as discussed in the context of TEM and XRD analysis of the high calcination temperature products. However, between 750 °C and 950 °C, absorptions in the near-ultraviolet region (380–435 nm) decreased slightly. We propose that under high temperatures, the mother ZnAl:LDH nanoplates were dismantled into nanoparticles (shown in Figs. 8 and 9), which led to a blue shift in the region.

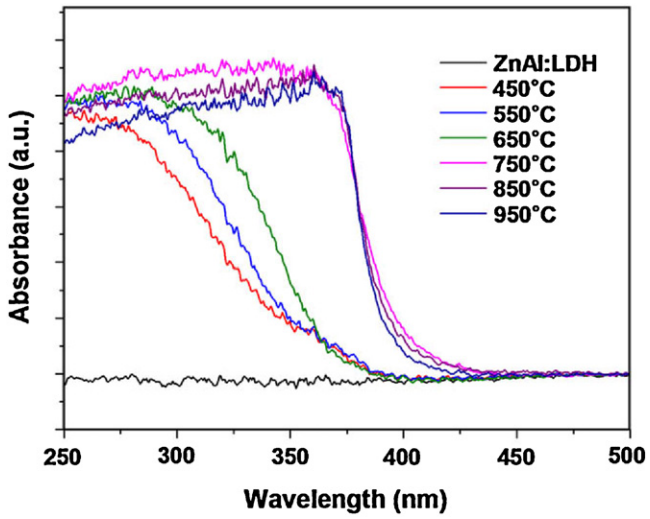

Fig. 10. UV–vis diffuse reflectance spectra of ZnAl:LDH nanostructures and their nanostructures produced by calcination at various temperatures.

4. Conclusions

In summary, we have presented a simple method for synthesizing ZnAl:LDH nanostructures at room temperature. HR-TEM analysis of the ZnAl:LDH nanostructures revealed that the crystal arrangements of the ZnAl:LDH nanostructures were unstable. Because the brucite-type layers were stacked and held together by hydrogen bonding, each layer could be easily moved and reconstructed under applied energy. Thus, the as-prepared ZnAl:LDH nanostructures could be converted into zinc aluminum MMO nanostructures by calcination in air. The crystalline natures and morphologies of the zinc aluminum MMO nanostructures could be controlled simply by varying the calcination temperature (from 450 °C to 950 °C). At low calcination temperatures, from 450 °C to 650 °C, the MMO nanostructures were composed of ZnO crystal and amorphous areas, and they were influenced by the crystal symmetry and orientations of the ZnAl:LDH nanostructures. The crystal orientations of the ZnO crystal grains were almost the same throughout the nanostructure. However, calcination above 750 °C produced $ZnAl_2O_4$ crystal grains, and amorphous regions could not be found in the MMO nanostructure. As the calcination temperature increased, the crystal grain size and surface roughness of the MMO nanostructures increased. Zinc aluminum MMO nanoparticles were obtained by calcination at 950 °C. ZnAl:LDH nanostructures and their calcined nanostructures were characterized by UV–vis diffuse reflectance spectroscopy. The spectra varied depending on the dimensions and crystalline natures of the MMO nanostructures. The present strategy and results may be applicable to the synthesis and expectation of crystalline natures of LDHs and MMOs with other metal combinations.

Acknowledgements

This work was supported by grants from the second phase BK21 program of the Ministry of Education of Korea and the Korea Science and Engineering Foundation (KOSEF) grant funded by the Korea government (MEST) (Grant No. 2011-0000360).

References

[1] A.P. Alivisatos, P.F. Barbara, A.W. Castleman, J. Chang, D.A. Dixon, M.L. Kline, G.L. McLendon, J.S. Miller, M.A. Ratner, P.J. Rossky, S.I. Stupp, M.I. Thompson, Adv. Mater. 10 (1998) 1297.
[2] L. Lu, Y. Shen, X. Chen, L. Qian, K. Lu, Science 304 (2004) 422.
[3] Y.S. Zhao, H. Fu, A. Peng, Y. Ma, D. Xiao, J. Yao, Adv. Mater. 20 (2008) 2859.
[4] A.N. Goldstein, C.M. Echer, A.P. Alivisatos, Science 256 (1992) 1425.
[5] M.A. Reed, W.R. Frensley, R.J. Matyi, J.N. Randall, A.C. Seabaugh, Appl. Phys. Lett. 54 (1989) 1034.
[6] P. Ball, L. Garwin, Nature 355 (1992) 761.
[7] M. Bruchez Jr., M. Moronne, P. Gin, S. Weiss, A.P. Alivisatos, Science 281 (1998) 2013.
[8] A. Corma, Chem. Rev. 97 (1997) 2373.
[9] W.B. Choi, E. Bae, D. Kang, S. Chae, B. Cheong, J. Ko, E. Lee, W. Park, Nanotechnology 15 (2004) S512.
[10] T. Yu, Y.W. Zhu, X.J. Xu, K.S. Yeong, Z.X. Shen, P. Chen, C.T. Lim, J.T.L. Thong, C.H. Sow, Small 2 (2006) 80.
[11] Z.Y. Fan, X.G. Wen, S.H. Yang, J.G. Lu, Appl. Phys. Lett. 87 (2005) 013113.
[12] J.C. Johnson, H. Yan, R.D. Schaller, P.B. Petersen, P. Yang, R.J. Saykally, Nano Letters 2 (2002) 279.
[13] Y. Wang, X. Xie, T. Goodson III, Nano Letters 5 (2005) 2379.
[14] H. Fan, Y. Lu, A. Stump, S.T. Reed, T. Baer, R. Schunk, V. Perez-Luna, G.P. López, C.J. Brinker, Nature 405 (2000) 56.
[15] P. Chauhan, S. Annapoorni, S.K. Trikha, Thin Solid Films 346 (1999) 266.
[16] R.F. Service, Science 287 (2000) 1902.
[17] Y. Kojima, K. Suzuki, Y. Kawai, J. Power Sources 155 (2006) 325.
[18] X. Fang, Y. Bando, U.K. Gautam, C. Ye, D. Golberg, J. Mater. Chem. 18 (2008) 509.
[19] C.S. Rout, A. Govindaraj, C.N.R. Rao, J. Mater. Chem. 16 (2006) 3936.
[20] G. Audoit, J.S. Kulkarni, M.A. Morris, J.D. Holmes, J. Mater. Chem. 17 (2007) 1608.
[21] C. Burda, X. Chen, R. Narayanan, M.A. El-Sayed, Chem. Rev. 105 (2005) 1025.
[22] Y. Cheng, Y. Wang, D. Chen, F. Bao, J. Phys. Chem. B 109 (2005) 794.
[23] Y. Jiang, X.-M. Meng, J. Liu, Z.-Y. Xie, C.-S. Lee, S.-T. Lee, Adv. Mater. 15 (2003) 323.
[24] J. Zhang, Q. Xu, Z.C. Feng, M.J. Li, C. Li, Angew. Chem. Int. Ed. 47 (2008) 1766.
[25] H.Y. Fan, K. Yang, D.M. Boye, T. Sigmon, K.J. Malloy, H.F. Xu, G.P. López, C.J. Brinker, Science 304 (2004) 567.
[26] A.P. Alivisatos, Science 271 (1996) 933.
[27] F. Cavani, F. Trifirò, A. Vaccari, Catal. Today 11 (1991) 173.
[28] P. Beaudot, M.E.D. Roy, J.P. Besse, Chem. Mater. 16 (2004) 935.
[29] J.T. Kloprogge, L. Hickey, R.L. Frost, J. Solid State Chem. 177 (2004) 4047.
[30] S.P. Newman, W. Jones, New J. Chem. (1998) 105.
[31] S. Hamada, K. Ikeue, M. Machida, Chem. Mater. 17 (2005) 4873.
[32] B. Mavis, M. Akinc, J. Power Sources 134 (2004) 308.
[33] J.H. Choy, S.Y. Kwak, Y.J. Jeong, J.S. Park, Angew. Chem. Int. Ed. 39 (2000) 4042.
[34] M.H. Huang, S. Mao, H. Feick, H. Yan, Y. Wu, H. Kind, E. Weber, R. Russo, P. Yang, Science 292 (2001) 1897.
[35] C. Liu, J.A. Zapien, Y. Yao, X. Meng, C.-S. Lee, S. Fan, Y. Lifshitz, S.-T. Lee, Adv. Mater. 15 (2003) 838.
[36] K. Yang, G.-W. She, H. Wang, X.-M. Ou, X.-H. Zhang, C.-S. Lee, S.-T. Lee, J. Phys. Chem. C 113 (2009) 20169.
[37] S. Cho, S.-H. Jung, K.-H. Lee, J. Phys. Chem. C 112 (2008) 12769.
[38] M.S. Arnold, P. Avouris, Z.W. Pan, Z.L. Wang, J. Phys. Chem. B 107 (2003) 659.
[39] S. Cho, S. Kim, N.-H. Kim, U.-J. Lee, S.-H. Jung, E. Oh, K.-H. Lee, J. Phys. Chem. C 112 (2008) 17760.
[40] Z.L. Wang, J.H. Song, Science 14 (2006) 242.
[41] H. Zeng, W. Cai, P. Liu, X. Xu, H. Zhou, C. Klingshirn, H. Kalt, ACS Nano 2 (2008) 1661.
[42] H. Zeng, X. Xu, Y. Bando, U.K. Gautam, T. Zhai, X. Fang, B. Liu, D. Golberg, Adv. Funct. Mater. 19 (2009) 3165.
[43] M. Zawadzki, J. Wrzyszcz, Mater. Res. Bull. 35 (2000) 109.
[44] X.Y. Chen, C. Ma, Z.J. Zhang, B.N. Wang, Mater. Sci. Eng. B 151 (2008) 224.
[45] X. Tiana, L. Wan, K. Pan, C. Tian, H. Fu, K. Shia, J. Alloys Compd. 488 (2009) 320.
[46] R. Pandey, J.D. Gale, S.K. Sampath, J.M. Recio, J. Am. Ceram. Soc. 82 (1999) 3337.
[47] S.K. Sampath, J.F. Cordaro, J. Am. Ceram. Soc. 81 (1998) 649.
[48] A.E. Galetti, M.F. Gomez, L.A. Arrúa, M.C. Abello, Appl. Catal. A: Gen. 348 (2008) 94.
[49] L.M. Chen, X.M. Sun, Y.N. Liu, K.B. Zhou, Y.D. Li, J. Alloys Compd. 376 (2004) 257.
[50] W.S. Tzing, W.H. Tuan, J. Mater. Sci. Lett. 15 (1996) 1395.
[51] L. Zou, F. Li, X. Xiang, D.G. Evans, X. Duan, Chem. Mater. 18 (2006) 5852.
[52] M.C. Marion, E. Garbowski, M. Primet, J. Chem. Soc. Faraday Trans. 11 (1991) 1795.
[53] L. Zou, X. Xiang, M. Wei, L. Yang, F. Li, D.G. Evans, Ind. Eng. Chem. Res. 47 (2008) 1495.
[54] N. Guilhaume, M. Primet, J. Chem. Soc. Faraday Trans. 11 (1994) 1541.
[55] M. Zawadzki, W. Mista, L. Kepinski, Vacuum 63 (2001) 291.
[56] X. Zhao, F. Zhang, S. Xu, D.G. Evans, X. Duan, Chem. Mater. 22 (2010) 3933.
[57] Y.W. Koh, M. Lin, C.K. Tan, Y.L. Foo, K.P. Loh, J. Phys. Chem. B 108 (2004) 11419.
[58] Y. Zhao, M. Wei, J. Lu, Z.L. Wang, X. Duan, ACS Nano 3 (2009) 4009.
[59] S. Cho, S.-H. Jung, J.-W. Jang, E. Oh, K.-H. Lee, Cryst. Growth Des. 8 (2008) 4553.
[60] M. Bellotto, B. Rebours, O. Clause, J. Lynch, D. Bazin, E. Elkaïm, J. Phys. Chem. 100 (1996) 8527.
[61] C. Jaubertie, M.J. Holgado, M.S. San Román, V. Rives, Chem. Mater. 18 (2006) 3114.
[62] K.-H. Goh, T.-T. Lim, Z. Dong, Water Res. 42 (2008) 1343.
[63] C.O. Oriakhi, I.V. Farrm, M.M. Lerner, J. Mater. Chem. 6 (1996) 103.
[64] N. Mameri, A.R. Yeddou, H. Lounici, D. Belhocine, H. Grib, B. Bariou, Water Res. 32 (1998) 1604.
[65] V. Prevot, C. Forano, J.P. Besse, F. Abraham, Inorg. Chem. 37 (1998) 4293.
[66] J. Zhang, F. Zhang, L. Ren, D.G. Evans, X. Duan, Mater. Chem. Phys. 85 (2004) 207.
[67] D.R. Hines, S.A. Solin, Phys. Rev. B 61 (2000) 11348.